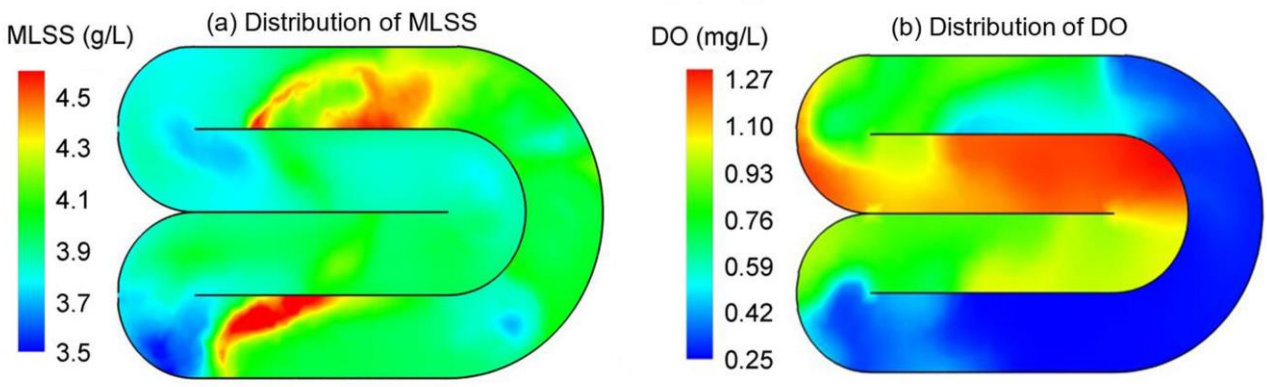

Figure S1. The distribution of: (a) MLSS concentration, 0.1 m above the bed; (b) DO concentration, 0.25 m above the bed in a pilot-scale oxidation ditch.

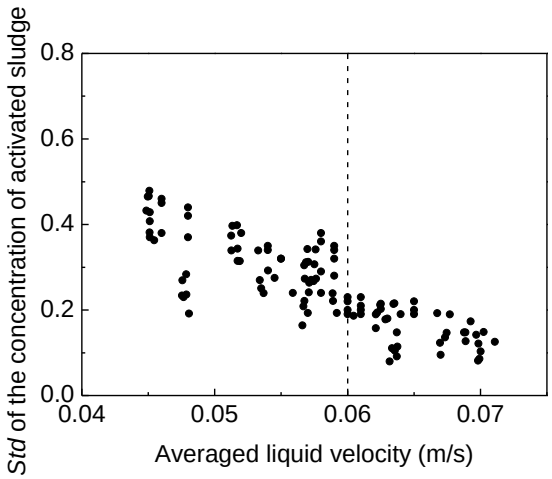

Figure S2. Correlation between averaged liquid velocity and standard deviation of MLSS concentration over a range of operational modes in a pilot-scale oxidation ditch.

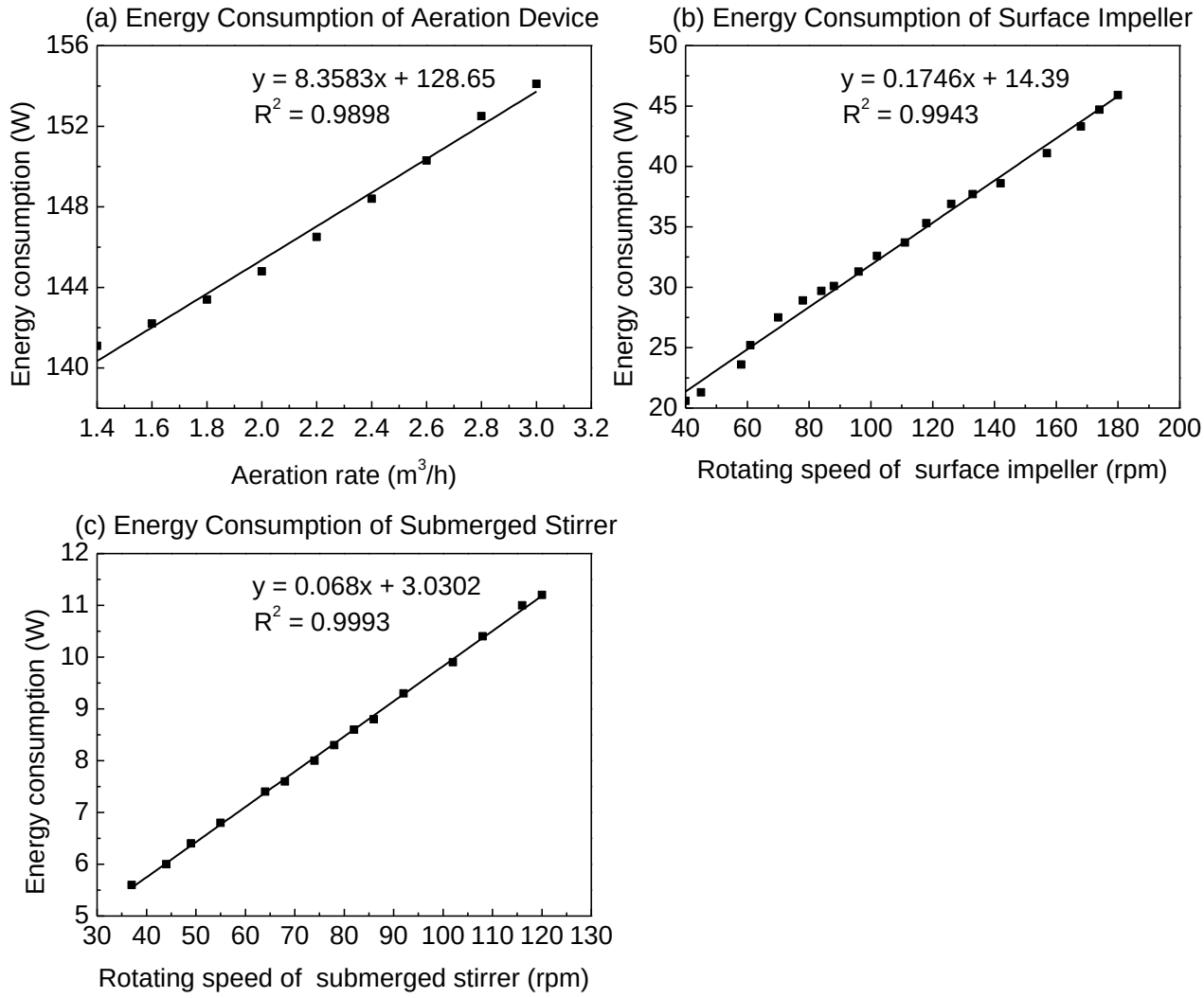

Figure S3. Energy consumption of: (a) aeration device, (b) surface impeller, and (c) submerged stirrer over the operational range of the pilot-scale OD.

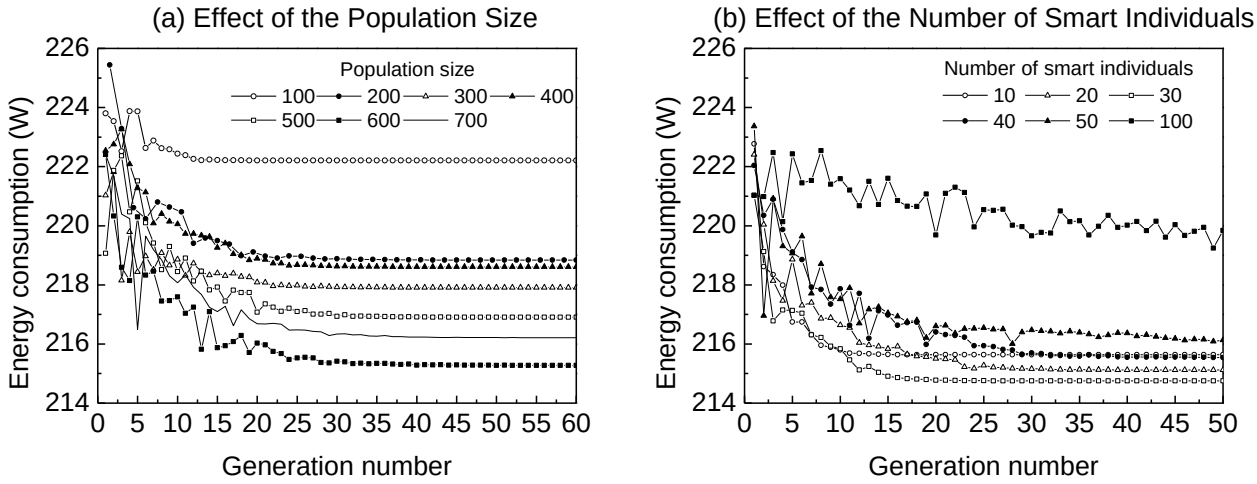

Figure S4. Effect of (a) population size and (b) number of smart individuals on the optimization results obtained by the AGA model for the pilot-scale OD.

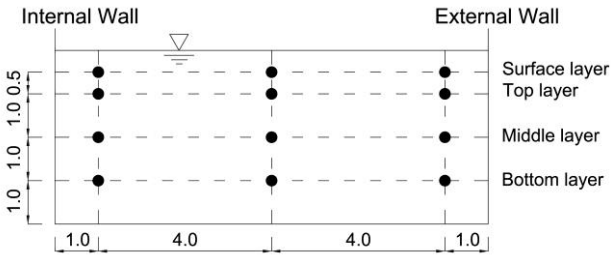

Figure S5. Sketch indicating sampling locations in the full-scale oxidation ditch at Ping Dngshan, Henan Province, China (Unit: m).

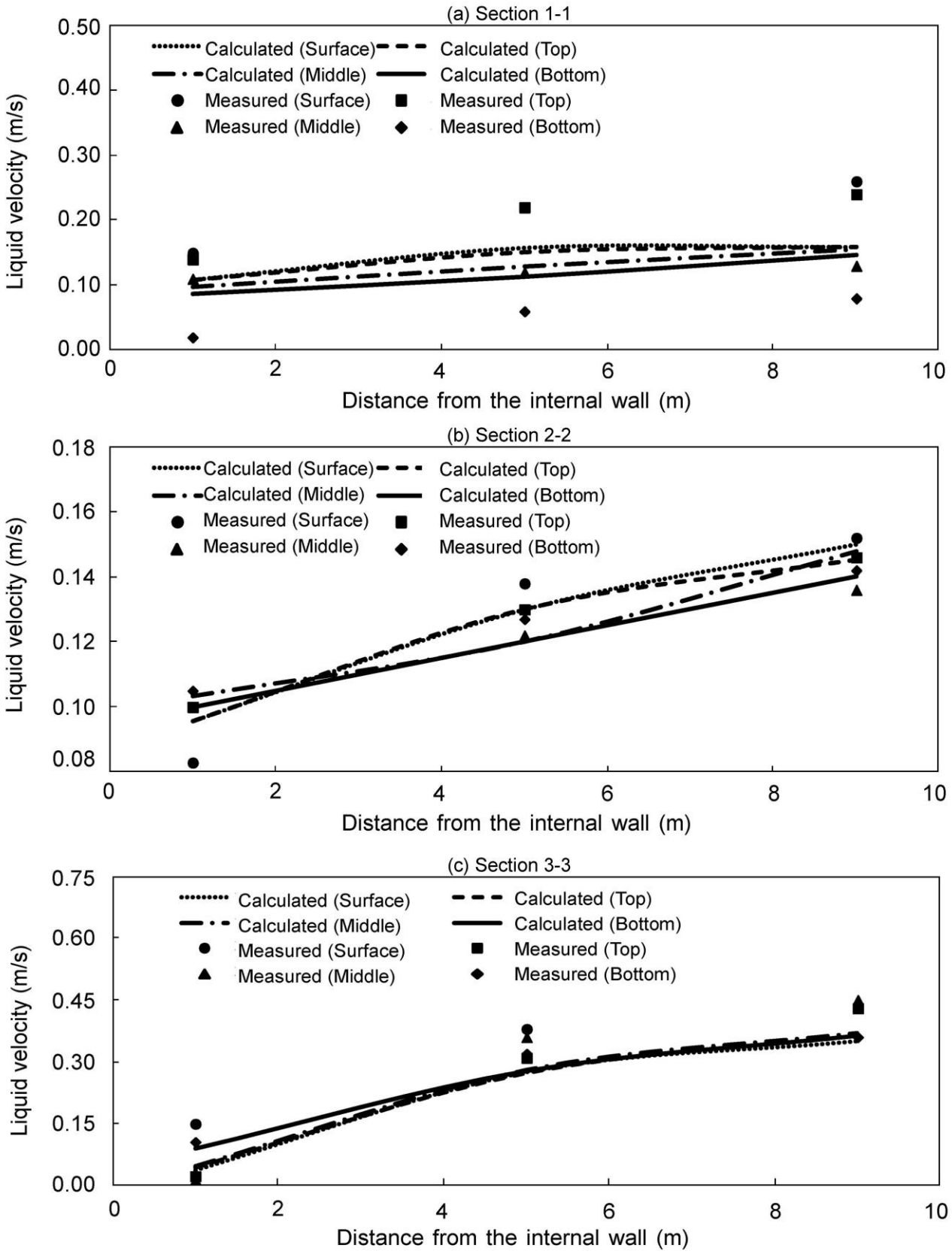

Figure S6. Predicted and measured transverse profiles under existing operating conditions of horizontal liquid speed across: (a) Section 1-1, (b) Section 2-2, and (c) Section 3-3 of the full-scale OD at Ping Dingshan, Henan Province, China.

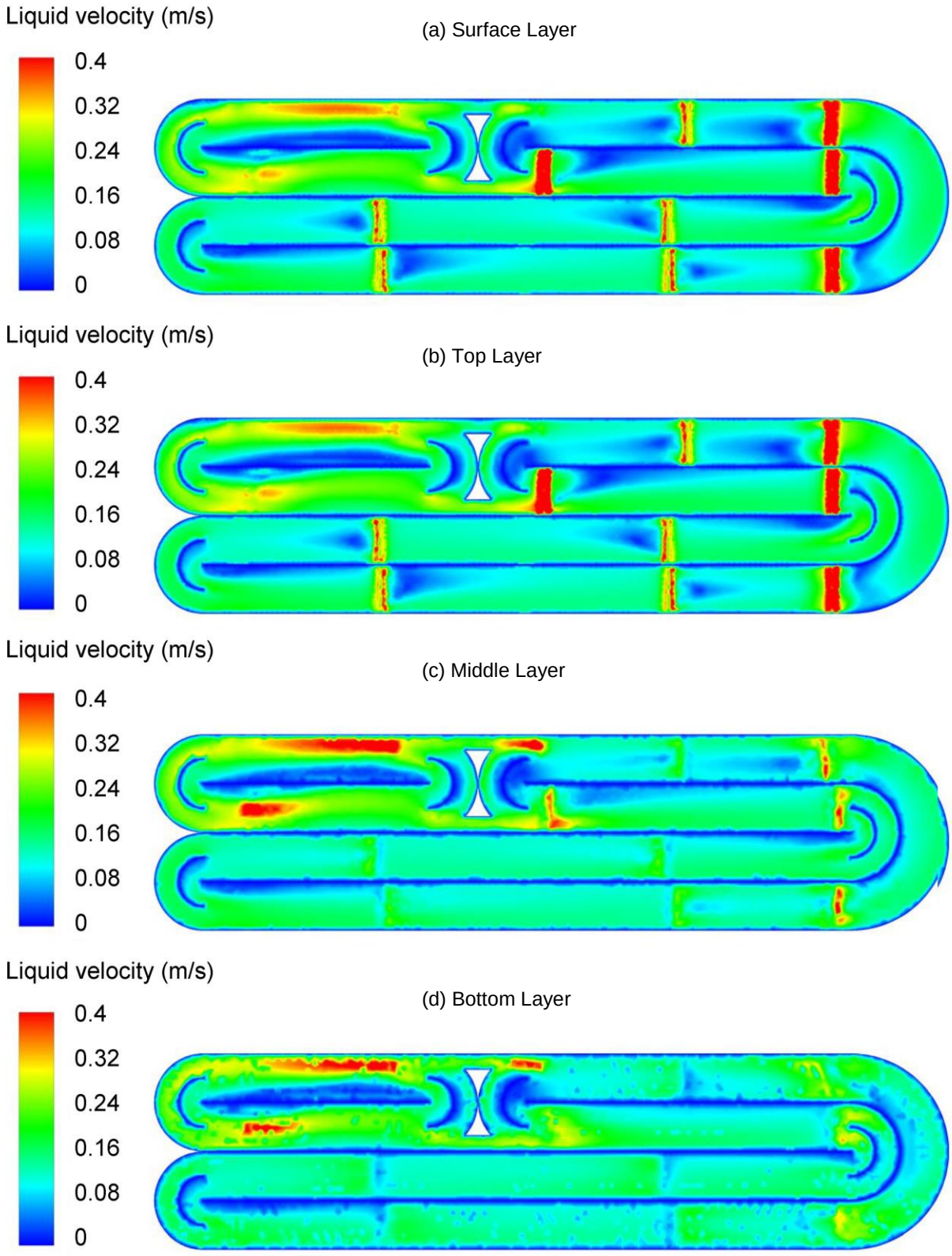

Figure S7. Predicted horizontal flow speeds in four horizontal slices through the depth: (a) surface layer, (b) top layer, (c) middle layer, and (d) bottom layer of the full-scale OD at Ping Dingshan, Henan Province, China.

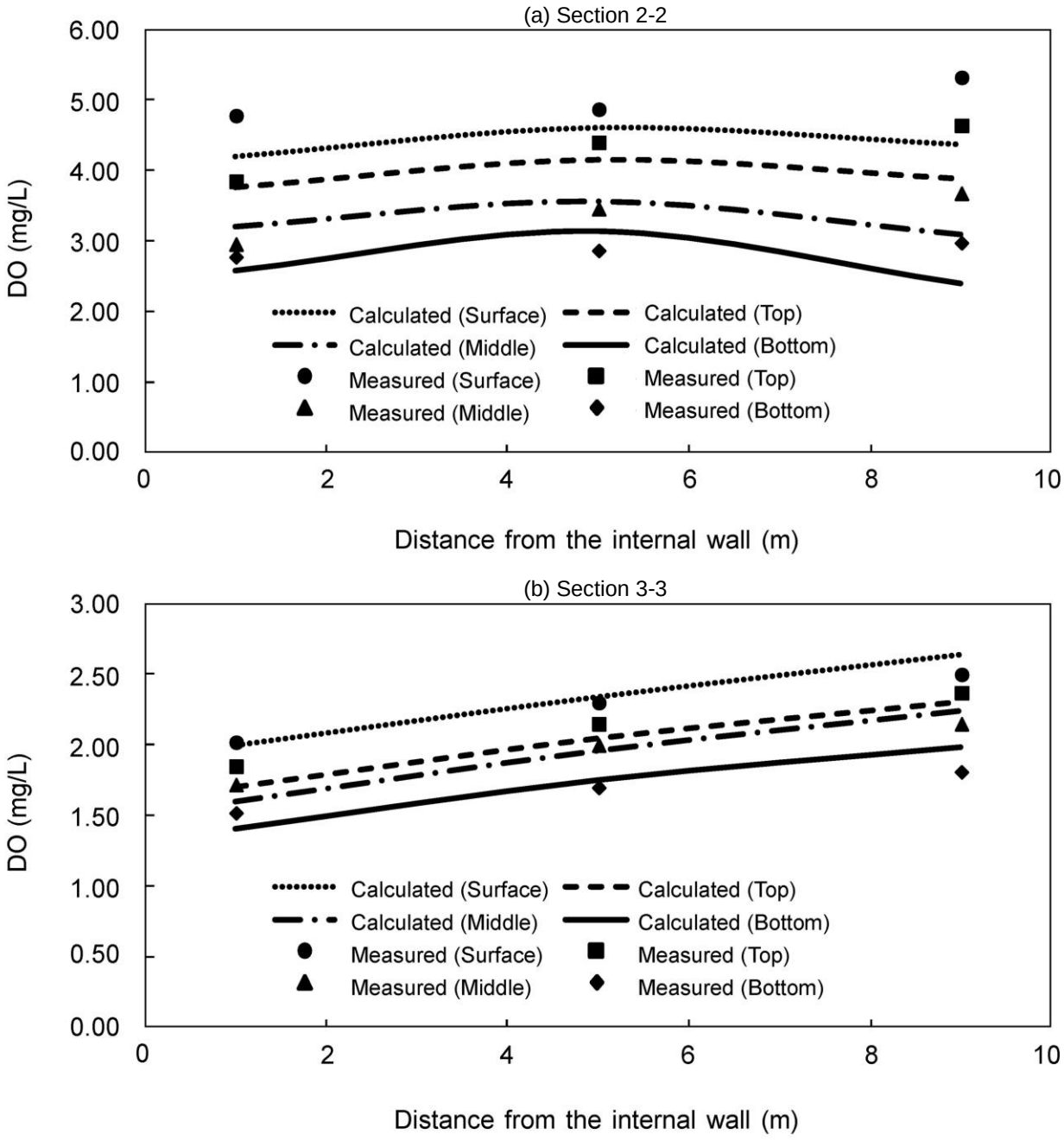

Figure S8. Simulated and measured dissolved oxygen concentration distributions at: (a) Section 2-2, and (b) Section 3-3 of the full-scale OD at Ping Dingshan, Henan Province, China.

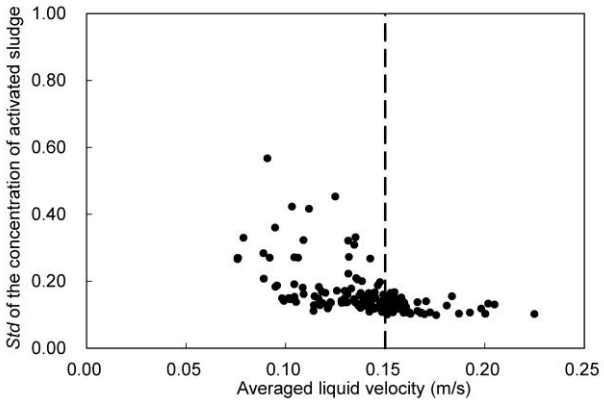

Figure S9. Correlation between average liquid velocity and standard deviation of MLSS concentration under different operation modes for the full-scale oxidation ditch at Ping Dingshan, Henan Province, China.